



Reconciling carbon quality with availability predicts temperature sensitivity of global soil carbon mineralization

Shuai Zhang^a , Mingming Wang^a , Liujuan Xiao^b , Xiaowei Guo^a , Jinyang Zheng^a , Biao Zhu^c , and Zhongkui Luo^{a,d,e,1}

Edited by William Schlesinger, Cary Institute of Ecosystem Studies, Millbrook, NY; received August 11, 2023; accepted January 22, 2024

Soil organic carbon (SOC) mineralization is a key component of the global carbon cycle. Its temperature sensitivity Q_{10} (which is defined as the factor of change in mineralization with a 10 °C temperature increase) is crucial for understanding the carbon cycle-climate change feedback but remains uncertain. Here, we demonstrate the universal control of carbon quality-availability tradeoffs on Q_{10} . When carbon availability is not limited, Q_{10} is controlled by carbon quality; otherwise, substrate availability controls Q_{10} . A model driven by such quality-availability tradeoffs explains 97% of the spatiotemporal variability of Q_{10} in incubations of soils across the globe and predicts a global Q_{10} of 2.1 ± 0.4 (mean \pm one SD) with higher Q_{10} in northern high-latitude regions. We further reveal that global Q_{10} is predominantly governed by the mineralization of high-quality carbon. The work provides a foundation for predicting SOC dynamics under climate and land use changes which may alter soil carbon quality and availability.

soil organic carbon | carbon pools | temperature sensitivity | mineralization | incubation

The mineralization of global soil organic carbon (SOC) results in the release of approximately 57 to 80 Pg C to the atmosphere as carbon dioxide (CO₂) each year (1, 2), equal to almost 9% of the atmospheric carbon pool. Climate warming may accelerate SOC mineralization (3), leading to positive soil carbon cycle-climate change feedbacks. However, the rate of this acceleration remains uncertain, particularly across large spatial extents (4, 5), and the underlying controls and mechanisms are also controversial (6, 7). According to the “carbon-quality temperature” hypothesis, recalcitrant SOC is more sensitive to temperature than labile SOC as it requires higher activation energy (8, 9), as depicted by the Arrhenius equation (10, 11). Nevertheless, comparable or even lower sensitivity of recalcitrant SOC has also been widely observed (12–14). This inconsistency could be explained by the low availability of SOC substrates to decomposers, mainly microbes. Indeed, the Michaelis–Menten theory predicts that if microbes cannot access substrates or are limited by metabolically preferred substrates (e.g., labile carbon with high energy density in order to utilize substrates with low energy density), SOC mineralization will be insensitive to temperature (15, 16). Physiochemical isolation of SOC from decomposition and other environmental constraints or unbalanced composition in terms of energy density and activation energy demand for overall SOC mineralization may result in general substrate limitation (17). Due to the high spatial heterogeneity of edaphic properties and high diversity of SOC composition, it is not surprising to observe highly variable apparent temperature sensitivity under different environmental conditions. Simultaneous consideration of carbon quality and availability is vital for reliable prediction of SOC mineralization in response to temperature changes (18).

We propose that combining the effects of carbon quality and availability can provide a universal explanation for the variability in the temperature sensitivity of SOC mineralization in global soils. Both factors affect the temperature sensitivity of SOC mineralization, but their relative importance depends on whether microbial mineralization is more limited by SOC quality or availability. This can be mathematically represented as (18): $Q_{10} = Q_{10_max} \cdot f(A) \cdot f(Q)$, where Q_{10} is the observed temperature sensitivity, defined as the change in SOC mineralization with a 10 °C temperature rise. Q_{10_max} represents the maximum potential Q_{10} , while $f(A)$ and $f(Q)$ (both range from 0 to 1) are the availability- and quality-limitation-induced reduction of Q_{10_max} , respectively (*Materials and Methods*). Specifically, if SOC availability is not or less limited [i.e., $f(A)$ is close to 1], Q_{10} is primarily limited by carbon quality [i.e., $f(Q) < f(A)$] with higher values under lower carbon quality, as predicted by the Arrhenius equation (Fig. 1). Conversely, if SOC availability is limited [i.e., $f(Q)$ is close to 1], carbon availability takes precedence [i.e., $f(Q) > f(A)$], resulting in lower Q_{10} under conditions of lower carbon availability, as predicted by the Michaelis–Menten equation (Fig. 1).

Significance

Understanding how soil carbon mineralization responds to warming is pivotal for accurate predictions of carbon cycle-climate change feedbacks and effective climate mitigation. By analyzing a comprehensive global dataset encompassing incubations of soils across the globe, we demonstrate that the temperature sensitivity of soil carbon hinges on the interplay between carbon quality and availability. In the absence of carbon limitations, carbon quality dictates sensitivity, with more recalcitrant carbon exhibiting higher temperature sensitivity. In situations of limited carbon availability, substrate availability becomes the decisive factor. Furthermore, we ascertain that temperature sensitivity of global soil carbon is primarily governed by the mineralization of labile carbon. Consequently, potential decline of labile carbon due to global warming may amplify positive carbon cycle-climate change feedbacks.

Author contributions: Z.L. designed research; S.Z. performed research; S.Z., M.W., L.X., and J.Z. analyzed data; S.Z. data collection; M.W. data collection and revised the manuscript; L.X., X.G., and J.Z. data collection and results interpretation; B.Z. data collection, revised the manuscript, and results interpretation; Z.L. revised the manuscript and led results interpretation; and S.Z., X.G., and B.Z. wrote the paper.

The authors declare no competing interest.

This article is a PNAS Direct Submission.

Copyright © 2024 the Author(s). Published by PNAS. This article is distributed under [Creative Commons Attribution-NonCommercial-NoDerivatives License 4.0 \(CC BY-NC-ND\)](https://creativecommons.org/licenses/by-nc-nd/4.0/).

¹To whom correspondence may be addressed. Email: luozk@zju.edu.cn.

This article contains supporting information online at <https://www.pnas.org/lookup/suppl/doi:10.1073/pnas.2313842121/-/DCSupplemental>.

Published March 4, 2024.

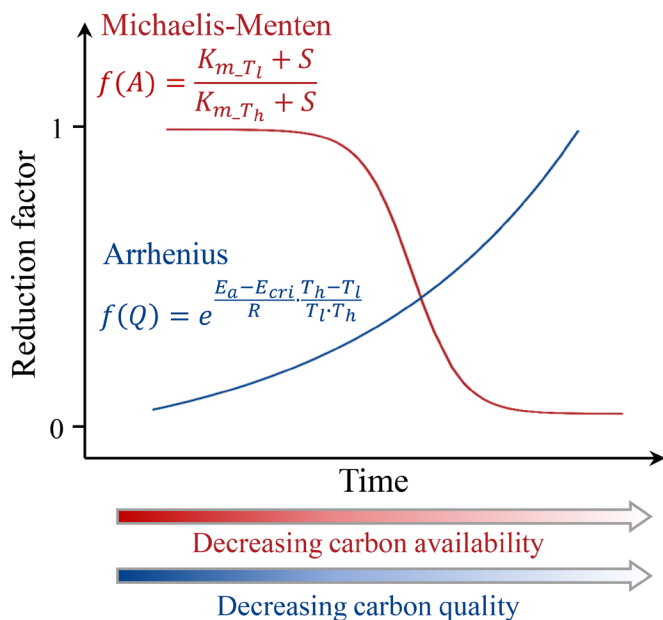


Fig. 1. Conceptual diagram of temperature sensitivity of soil carbon mineralization (Q_{10}) as impacted by substrate quality and availability. The effects of substrate availability [$f(A)$] and quality [$f(Q)$] are depicted by the Michaelis–Menten and Arrhenius equations, respectively. Parameters in the equations are elucidated in *SI Appendix, Table S2*.

To test our proposition, we conducted a comprehensive literature review and obtained a global dataset of SOC mineralization from 721 soils collected worldwide (*SI Appendix, Fig. S1*) under laboratory incubation conditions. We used a continuous interval of 0.2% to calculate the mineralized fraction, which indicates a decreasing gradient of SOC quality and availability over the course of incubation. Then, we estimated changes in the Q_{10} of SOC mineralization over time by calculating the “equal-carbon” Q_{10} (19, 20) based on the time required to respire a defined fraction of SOC (0 to 0.2%, 0.2 to 0.4%, 0.4 to 0.6%, etc.). As incubation experiments typically do not involve continuous carbon inputs, the respired fraction provided an opportunity to distinguish between quality- and availability-limited Q_{10} by evaluating the temporal dynamics of Q_{10} with the progression of incubation (e.g., depletion of labile SOC and decrease of SOC availability). Using the calculated temporal Q_{10} values and their corresponding respired fractions, we fitted a model based on the proposed interactions between carbon quality and availability to assess whether the model can accurately capture the temporal dynamics of observed Q_{10} , and the model was applied to infer Q_{10} at the start of incubation ($Q_{10, \text{initial}}$) and the relative importance of carbon quality and quantity.

Results and Discussion

Two Theoretical Types of Temporal Q_{10} Dynamics. If our proposition regarding the interactions between carbon quality and availability is correct, and the incubation period is long enough, we would only observe two types of temporal Q_{10} dynamics characterized by decreased carbon quality and availability as incubation progresses. Type I involves an initial increase in Q_{10} to a maximum, followed by a decrease (i.e., an increase phase followed by a decrease phase). For this type, the initial substrate is sufficient, and mineralization is not limited. The initial Q_{10} and the rate of change toward the turning point would vary depending on the initial substrate quality. However, depending on the initial

substrate availability and the length of the incubation, we may only observe the first increase phase (*SI Appendix, Fig. S2A*). Type II involves a persistent decrease in Q_{10} , regardless of incubation duration, due to persistent availability limitations (*SI Appendix, Fig. S2B*). The initial Q_{10} and the rate of decrease depend on the initial intensity of the limitation. These expectations have been confirmed. Specifically, 77% of the trials can be clearly classified into these two types (*SI Appendix, Supplementary Data*). Among them, 65% are type I, which on average have a higher initial SOC content (i.e., lower probability of substrate limitation) than type II trials (6.5 % vs. 3.3 %, *SI Appendix, Fig. S3*) which accounts for 12% of the trials (*SI Appendix, Supplementary Data*). We compared the maximum Q_{10} values among the two types (*SI Appendix, Fig. S4*). The maximum Q_{10} values were expected to be in an order of type I > type II, which was confirmed in our analysis. On average, the maximum Q_{10} value in Type I trials was 3.9, which was almost as twice as the maximum Q_{10} value in Type II trials (*SI Appendix, Fig. S4*).

There are 23% of the trials that do not fall into either type I or type II categories and are referred to as type III dynamics. In these trials, Q_{10} either remains stable or fluctuates greatly over time (*SI Appendix, Fig. S2C*). The reason for such dynamics may be due to several factors such as the presence of abundant substrates with similar quality and/or activation energy, very low carbon availability, and unstable incubation environment, among others. Upon examining these trials, we found that they tended to have short pre-incubation periods (which may not allow for microbial stabilization), or larger temperature differences for estimating Q_{10} (which may result in complex consequences on microbial metabolisms and carbon use strategies).

Spatiotemporal Variability of Q_{10} and Its Drivers. Individual Q_{10} values estimated from the global dataset vary substantially among soils and over time, ranging from 0.1 to 15 with a median of 1.8 (Q_{10} values exceeding 15, which accounts for 1% of the total data and may be caused by confounding factors such as microbial community shifts, enzyme responses, and desorption of carbon substrates from mineral surfaces (21, 22), have been excluded in this study, Fig. 2A). This spatiotemporal variability of Q_{10} is well explained ($R^2 = 0.94$) by a machine learning–based model—random forest—driven by climatic, vegetation and edaphic properties at the soil location, incubation manipulation, and respired fraction of SOC (Fig. 2A). Respired fraction alone explains 33% of the variance of Q_{10} (Fig. 2B). As the calculated time-course values of respired fraction are proxies of carbon quality and availability, this result demonstrates the critical role of carbon quality and availability in controlling Q_{10} . Mean annual temperature at soil location and two incubation manipulation-related variables including incubation temperature range and the lower temperature to estimate Q_{10} are the following three most important variables, explaining 5%, 6%, and 5% of the Q_{10} variance, respectively. All other variables assessed have less than 5% interpretability (*SI Appendix, Fig. S5*). Together, incubation manipulation explains 24% of the variance of Q_{10} , while climatic and edaphic properties explain 15% and 22% of the variance of Q_{10} , respectively. Vegetation variables together only explain 6% (*SI Appendix, Fig. S5*). These findings demonstrate the integrated effects of environmental conditions and experimental manipulation on Q_{10} estimation and explain why Q_{10} varies greatly in the literature.

Averaging across the globe dataset, Q_{10} initially increases and then decreases as incubation progresses, in conjunction with the increase of the respired fraction of SOC (*SI Appendix, Fig. S6*). The average Q_{10} at the turning point, where it transitions from

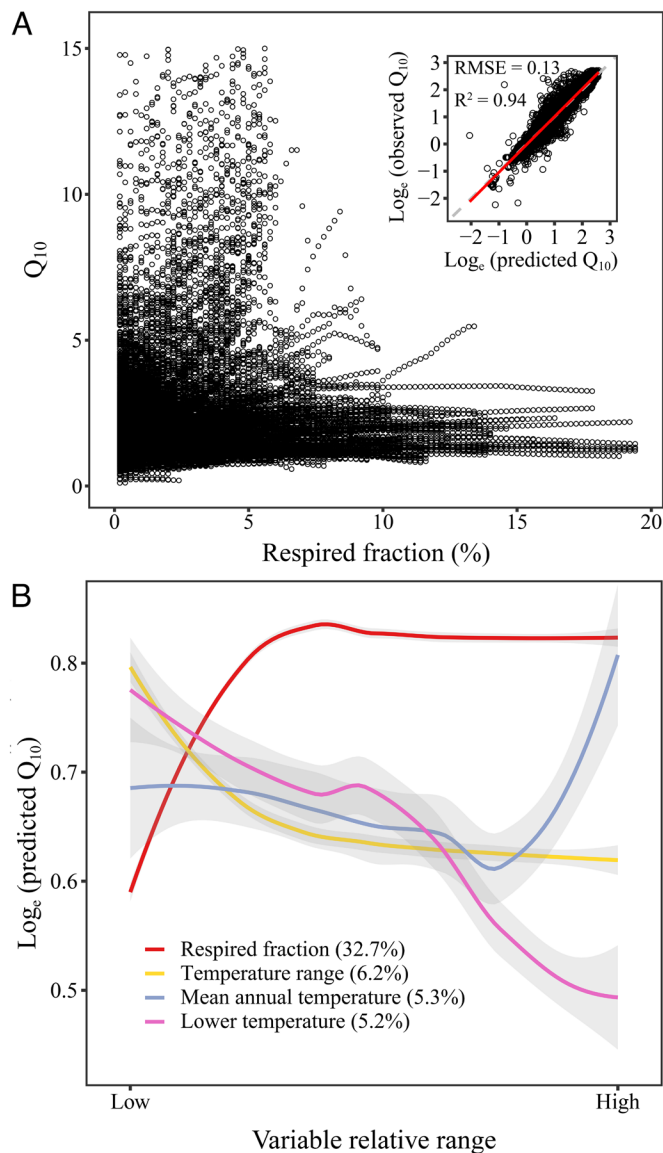


Fig. 2. Spatiotemporal changes in the temperature sensitivity of soil carbon mineralization (Q_{10}) and their main drivers. Q_{10} values were calculated for cumulative respired fractions at an interval of 0.2% (0 to 0.2%, 0.2 to 0.4%, 0.4 to 0.6%, etc.). (A) Variation of Q_{10} values with respired fraction. Inset shows the performance of a random forest model to explain the variance of Q_{10} values, gray dashed line shows the 1:1 line, and red line shows the regression line. RMSE, root mean squared error; R^2 , determination coefficient. (B) Partial dependence of Q_{10} values on the four most important controlling factors which explain 5% variance of Q_{10} at least. Shading area shows the 95% CI. Temperature range is the difference of two temperatures used to calculate Q_{10} , and lower temperature is the low temperature of the range.

increase to decrease, is 3.1 (which represents an average maximum Q_{10}). At this point, the corresponding respired fraction of SOC ranges between 4.2 and 4.4%. When we divide the data into two groups with and without carbon inputs, the group with carbon inputs shows a smaller Q_{10} of 2.6 at the turning point, with the corresponding respired fraction of SOC increasing to 4.8 to 5.0% (SI Appendix, Fig. S6), suggesting that the addition of new carbon delays Q_{10} from reaching its maximum. The global average temporal pattern of Q_{10} suggests interactive effects of carbon quality and availability on the temperature sensitivity of SOC. In the first phase, Q_{10} increases with incubation due to the depletion of labile SOC until reaching the turning point, while in the second phase, Q_{10} shows a decreasing trend (SI Appendix, Fig. S6). Notably,

many laboratory incubation experiments observed only the increase phase of Q_{10} (19, 23, 24), likely due to abundant substrates or the relatively short duration of the incubation as discussed above.

Interactions between Carbon Quality and Availability. The global average temporal dynamics of Q_{10} can be well captured ($R^2 = 0.89$) by modeling the interactions between carbon quality and availability (Fig. 3A). Examining the two reduction factors, $f(Q)$ and $f(A)$, which represent the effects of carbon quality and availability, respectively, it is evident that the initial increase phase is primarily controlled by $f(Q)$ while $f(A)$ is larger and closer to 1 than $f(Q)$, and the subsequent decrease phase is primarily controlled by $f(A)$ while $f(Q)$ remains relatively stable and close to 1 (Fig. 3B). The model explains 97% of the spatiotemporal variance of Q_{10} across the trials (Fig. 3C). For individual trials, the model explains >50% of the Q_{10} variance in 88% trials (SI Appendix, Fig. S7). Trials with relatively poor model performance mainly belong to type III trials with large fluctuations in Q_{10} over time (SI Appendix, Figs. S7 and S8). For type III trials, the model explains 94% of the Q_{10} variance, but the RMSE (root mean squared error) is larger than that of type I and type II trials (Fig. 3C). However, it is interesting to note that the average Q_{10} of type III trials also presents clear type I dynamics (Fig. 3A), supporting the general global pattern of the two phases albeit potential confounding factors in individual trials.

The modeling results provide critical insights into the interactions between substrate availability (S) and quality indicated by activation energy (E_a) in regulating Q_{10} (Materials and Methods). Theoretically, if microbial mineralization is not limited by S, Q_{10} should be equal to the maximum potential Q_{10} (i.e., Q_{10_max} in the model) which is inherently determined by substrate chemistry (22). In this case, the Michaelis–Menten equation models a constant Q_{10} and is incapable of simulating the determinant process underpinning Q_{10_max} and therefore Q_{10} . Simulation of carbon quality represented by the Arrhenius equation compensates such incapability and simulates Q_{10} as a function of E_a of substrates under sufficient S. At the beginning of the trials, specifically, E_a (i.e., E_0 in the model) was estimated to have a mean value of $51.1^{209.8}_{2.4}$ kJ mol⁻¹ (mean with 5% and 95% quantiles) (SI Appendix, Fig. S9). This range of values encompasses a number of empirical observations and theoretical estimates of E_a obtained under various soil environmental conditions (9, 25, 26). When mineralization is limited by S, Q_{10} is jointly regulated by S and E_a . Although low-quality substrates have a higher E_a and thus a higher Q_{10} , decomposers will be eventually limited by energy availability for activating the mineralization of recalcitrant SOC (27). These evaluations have been verified by comparing the distributions of optimized model parameters among the three types of trials (SI Appendix, Fig. S9). First, Q_{10_max} is on average comparable among the three types (SI Appendix, Fig. S9A). Second, except E_0 , all parameters are significantly different between type I and type II trials, while these parameters for type II trials either significantly differ from type I trials or from type II trials (SI Appendix, Fig. S9 B and C). For example, it is expected that the magnitude of initial substrate availability (S_0) at the beginning of Type I trials is greater than that of type II trials. These results align with our proposition that the three types of trials may present distinct status in terms of carbon quality or carbon availability.

Initial Q_{10} and Its Global Pattern. In the Q_{10} model, the effects of both carbon quality $f(Q)$ and availability $f(A)$ are modeled as functions of respired fraction (Materials and Methods), allowing us

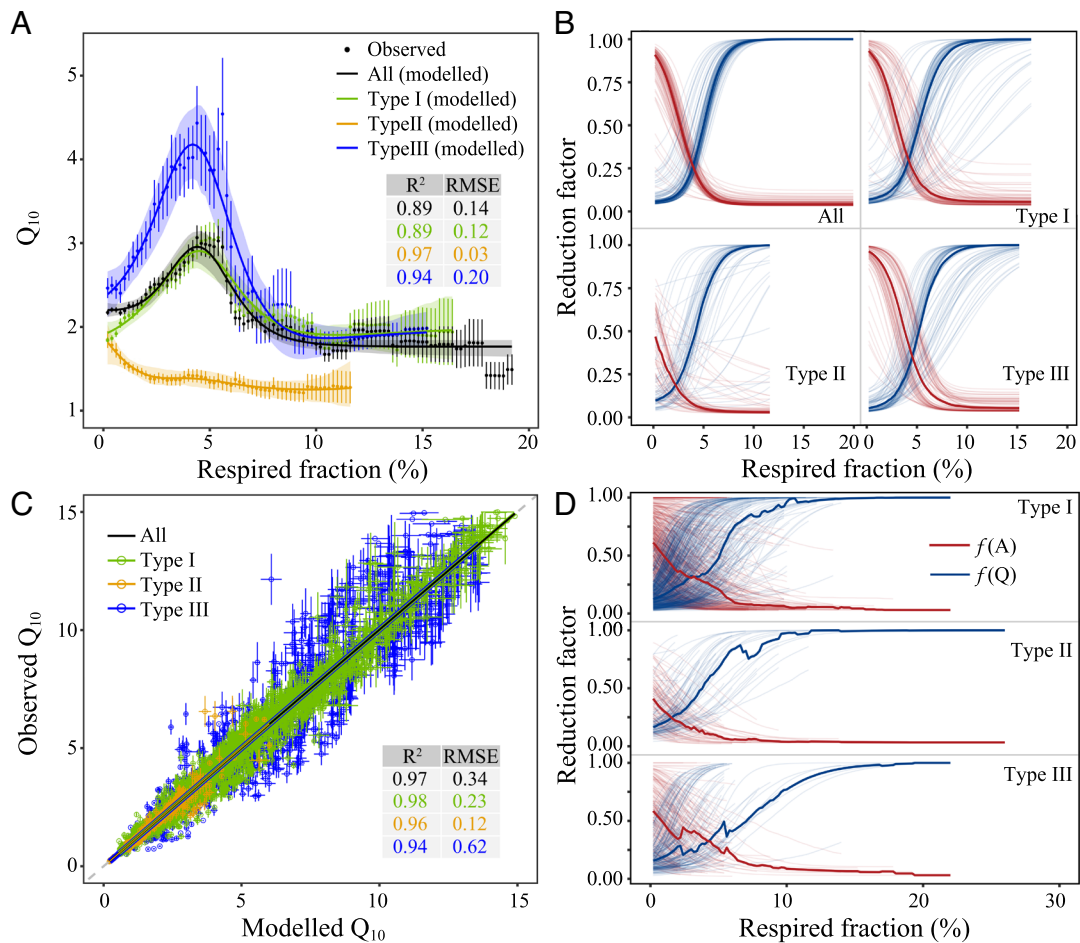


Fig. 3. Observed and modeled temperature sensitivity of soil carbon mineralization (Q_{10}). (A) Model performance for predicting the temporal variability of global mean Q_{10} . Shading area represents the 95% CI of the simulation, solid line shows the median of the 200 simulations. Bars represent one SE of observations. Type I shows that Q_{10} first increases and then decreases with time. Type II represents a persistent decrease in Q_{10} . Type III shows that the temporal dynamic of Q_{10} do not fall into either type I or type II categories. (B) The temporal dynamics of fitted $f(A)$ and $f(Q)$ values corresponding to the Q_{10} in (A). Thin lines show 200 estimates considering uncertainties in the data, and bold lines show the median of the 200 estimates. (C) Model performance by pooling individual results together. Vertical and horizontal bars represent one SDs of observed and modeled values, respectively. Gray dashed line shows the 1:1 line, and solid line shows the regression line. (D) the temporal dynamics of $f(A)$ and $f(Q)$ values for the three types. RMSE, root mean squared error; R^2 , determination coefficient. Thin lines show the median of 200 estimates for each individual trial, and bold lines show the mean value of the medians for each type of trials.

to estimate initial $f(Q)$, $f(A)$, and thus Q_{10} at the start of incubation by setting the respired fraction to zero which are, respectively, referred as $f(Q)_{\text{initial}}$, $f(A)_{\text{initial}}$, and $Q_{10_{\text{initial}}}$ hereafter. These initial values can help diagnose $f(Q)$, $f(A)$, and Q_{10} under field conditions, assuming that soil carbon quality and availability at the start of incubation can approximate that in the field.

The optimized Q_{10} model estimates a $Q_{10_{\text{initial}}}$ of 1.9 ± 1.1 (mean \pm one SD), with the highest $Q_{10_{\text{initial}}}$ in tundra (3.3 ± 1.8), followed by cropland (2.2 ± 1.3), forest (1.9 ± 1.1), and wetland (1.8 ± 0.5). Grassland exhibits the lowest $Q_{10_{\text{initial}}}$ of 1.5 ± 0.5 (Fig. 4A). We compare our estimates of $Q_{10_{\text{initial}}}$ for soil incubation with that based on field observations of total soil ($Q_{10_{\text{Rs}}}$) and heterotrophic respiration ($Q_{10_{\text{Rh}}}$) (28). The results show that the average $Q_{10_{\text{initial}}}$ for soil incubation across the globe is generally smaller than $Q_{10_{\text{Rh}}}$ (2.2 ± 0.6) which is significantly smaller than $Q_{10_{\text{Rs}}}$ (2.5 ± 0.8 , Fig. 4A). While $Q_{10_{\text{initial}}}$ and $Q_{10_{\text{Rh}}}$ are comparable in grasslands, $Q_{10_{\text{initial}}}$ is consistently smaller than $Q_{10_{\text{Rs}}}$ irrespective of ecosystems. These discrepancies would be attributed to factors such as 1) different approaches used to estimate Q_{10} (i.e., no model can 100% explain the data), 2) model-fitting uncertainties due to data quantity and quality limitations, and 3) inconsistent representativeness of the datasets

for estimating the three Q_{10} metrics. Despite the discrepancies, it is important to note that all three Q_{10} metrics (especially $Q_{10_{\text{initial}}}$) show large variability (Fig. 4A), and $Q_{10_{\text{initial}}}$ values less than 1 are not rare. These results highlight the importance of assessing context-dependent Q_{10} and suggest that warming does not necessarily accelerate SOC mineralization (29). The consistently higher $Q_{10_{\text{Rs}}}$ compared to $Q_{10_{\text{Rh}}}$ and $Q_{10_{\text{initial}}}$ may be due to temperature-dependent root growth and biomass which directly influence the total amount of root respiration and thus the estimation of $Q_{10_{\text{Rs}}}$ (30).

The variability of $Q_{10_{\text{initial}}}$ can be reasonably predicted (cross-validation $R^2 = 0.76$) by a random forest model driven by climatic, edaphic, and vegetation properties (*SI Appendix, Fig. S10*). We apply the random forest model to predict $Q_{10_{\text{initial}}}$ for each 1-km grid across the globe (Fig. 5). The global average $Q_{10_{\text{initial}}}$ is 2.1 (Fig. 5A and B), which is consistent with another study (28). Digital global mapping shows higher temperature sensitivity of SOC mineralization in northern high-latitude regions (Fig. 5B). The most sensitive areas are located in northern Alaska, northern Canada, and central and eastern Siberia which also have high soil carbon content. Some arid/semi-arid tropical regions, such as northern sub-Saharan Africa and northern regions

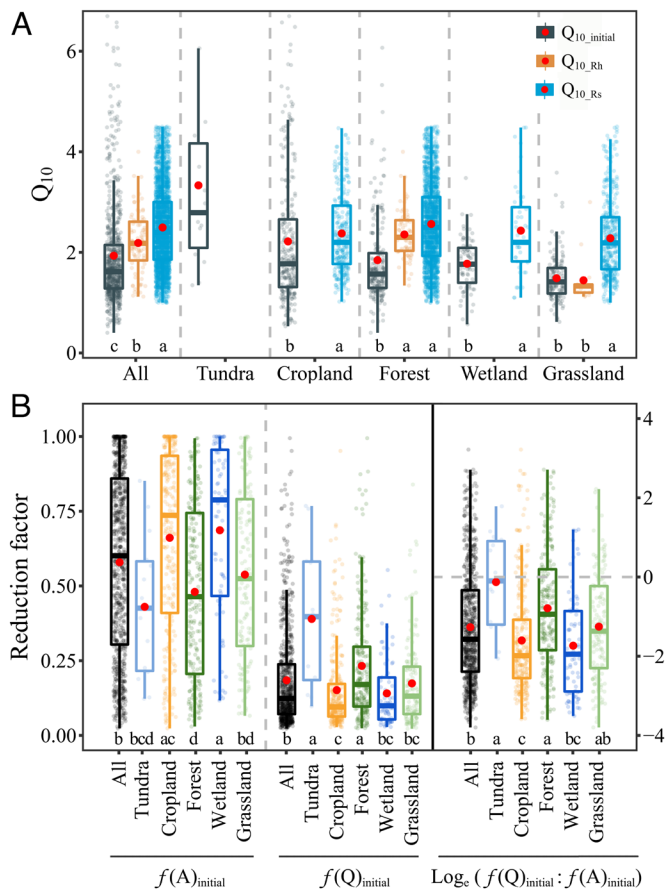


Fig. 4. Inferred temperature sensitivity of soil carbon mineralization at the start of incubation ($Q_{10_initial}$) and the impacts of carbon availability [$f(A)_{initial}$] and quality [$f(Q)_{initial}$]. Q_{10_Rh} , Q_{10_Rs} are the Q_{10} of soil heterotrophic and total respiration (heterotrophic plus autotrophic respiration), respectively, and are derived from ref. 28. Values of <1 and >4.5 are excluded in ref. 28. Red dots show the mean value. Different letters in (A) represent a significant difference among the estimates at the level of $P < 0.05$. Different letters in (B) represent a significant difference among ecosystems at the level of $P < 0.05$. The left y-axis in (B) represents the value of reduction factor [i.e., $f(A)_{initial}$ and $f(Q)_{initial}$] and the right y-axis represents the value of $\log_e [f(Q)_{initial} : f(A)_{initial}]$.

of the Namib Desert, also have high $Q_{10_initial}$. However, the data in these regions are very limited (SI Appendix, Fig. S1), which would be also the reason of larger uncertainty compared to other regions (Fig. 5 C and D).

The Relative Importance of Carbon Quality and Availability.

The estimated $f(Q)_{initial}$ and $f(A)_{initial}$ values provide crucial insights into the relative significance of carbon quality and availability in governing $Q_{10_initial}$. Across the incubated soils, on average $f(Q)_{initial}$ is smaller than $f(A)_{initial}$, with an average log ratio of $f(Q)_{initial}$ to $f(A)_{initial}$ of -1.3 (Fig. 4B). This suggests that substrate quality exerts a stronger influence than availability in limiting $Q_{10_initial}$. That is, SOC mineralization is dominant by relatively labile SOC components with lower activation energy, and quality limitation of Q_{10} would be more common than availability limitation in global soils.

However, tundra soils are different from soils in other ecosystems, as they are much less limited by quality, and the importance of quality and availability is comparable with an average log ratio of $f(Q)_{initial}$ to $f(A)_{initial}$ of -0.1 (Fig. 4B). Although Arrhenius kinetics predict higher $f(Q)$ for a given carbon quality at lower temperatures, this can be explained by two other factors. On the one hand, carbon availability in tundra for microbial decomposition

is often limited by low temperature as most SOC is frozen in peat for most of the year (e.g., permafrost). On the other hand, high-quality carbon substrates with high nutrient content (e.g., nitrogen) are usually scarce in tundra soils (31–33). It has been suggested that tundra soils are often dominated by complex carbon compounds, such as lignin, cellulose, and hemicellulose, which are difficult for microbes to decompose due to nutrient limitation (33). As a result, the Q_{10} of SOC mineralization in tundra may be vulnerable to shifts in both quality and availability, while Q_{10} of other ecosystems would be more sensitive to quality changes. Wetland soils show the smallest log ratios of $f(Q)_{initial}$ to $f(A)_{initial}$ (Fig. 4B). For wetland soils, they are usually carbon-rich due to inhibited SOC decomposition under anaerobic conditions and therefore have a low probability of availability limitation. Additionally, waterlogging promotes the formation of dissolved SOC, which can be more bioavailable to decomposers and typically has a high quality (34).

It is worth noting that most soil incubations are conducted under optimal soil moisture conditions. Since soil moisture is a critical factor influencing the accessibility of carbon to microbes, incubation data may underestimate the impact of carbon availability on Q_{10} if optimal soil moisture conditions alleviate the constraints on carbon availability (35). In real field conditions, both drought and waterlogging (as observed in wetland soils) can limit microbial access to or utilization of carbon substrates, subsequently affecting the apparent Q_{10} . Additionally, other aspects of incubation procedures, such as the duration of pre-incubation and soil sieving, can influence the stabilization and destabilization processes of soil carbon, as well as microbial activities. These factors may impact the temporal dynamics of Q_{10} .

Conclusions and Implications

Our results demonstrate that carbon quality–availability interactions universally control the temperature sensitivity of SOC mineralization across the globe and over time. This interaction can be effectively modeled by integrating Arrhenius and Michaelis–Menten kinetics. When mineralization is not limited by substrates, carbon quality explains the increasing Q_{10} values as SOC quality declines. Conversely, when substrates are limited, Q_{10} decreases with decreasing availability. The estimated Q_{10} across the globe is 2.1 with much higher values in colder regions. Furthermore, we found that carbon quality plays a predominant role in controlling Q_{10} globally. High-quality SOC may contribute to the majority of global SOC mineralization (36), and the sensitivity of SOC to warming may significantly rise if warming results in depletion of high-quality SOC, i.e., positive soil carbon cycle–climate change feedbacks. However, on a global scale, 4% SOC loss would result in availability limitation-induced decrease of Q_{10} .

The carbon quality–availability interactions can serve as a foundation for explaining or inferring whole-profile SOC dynamics in response to changes in carbon quality and availability. Climate and land management changes may alter carbon inputs to soils in terms of both quality and quantity (37), thereby changing SOC quality and availability. The consequences of such changes will depend on the temporal dynamics of carbon quality and availability and their interactions. A long-term field warming experiment has observed multi-phase decay of SOC (13), which can be explained by the shifts in carbon substrate quality and availability during the experiment. Based on the general vertical distribution of carbon quality and availability (38), it is reasonable to infer that topsoil SOC dynamics would be more sensitive to quality changes as topsoil is generally substrate-abundant and has high-quality substrates, while subsoil SOC is more sensitive to availability

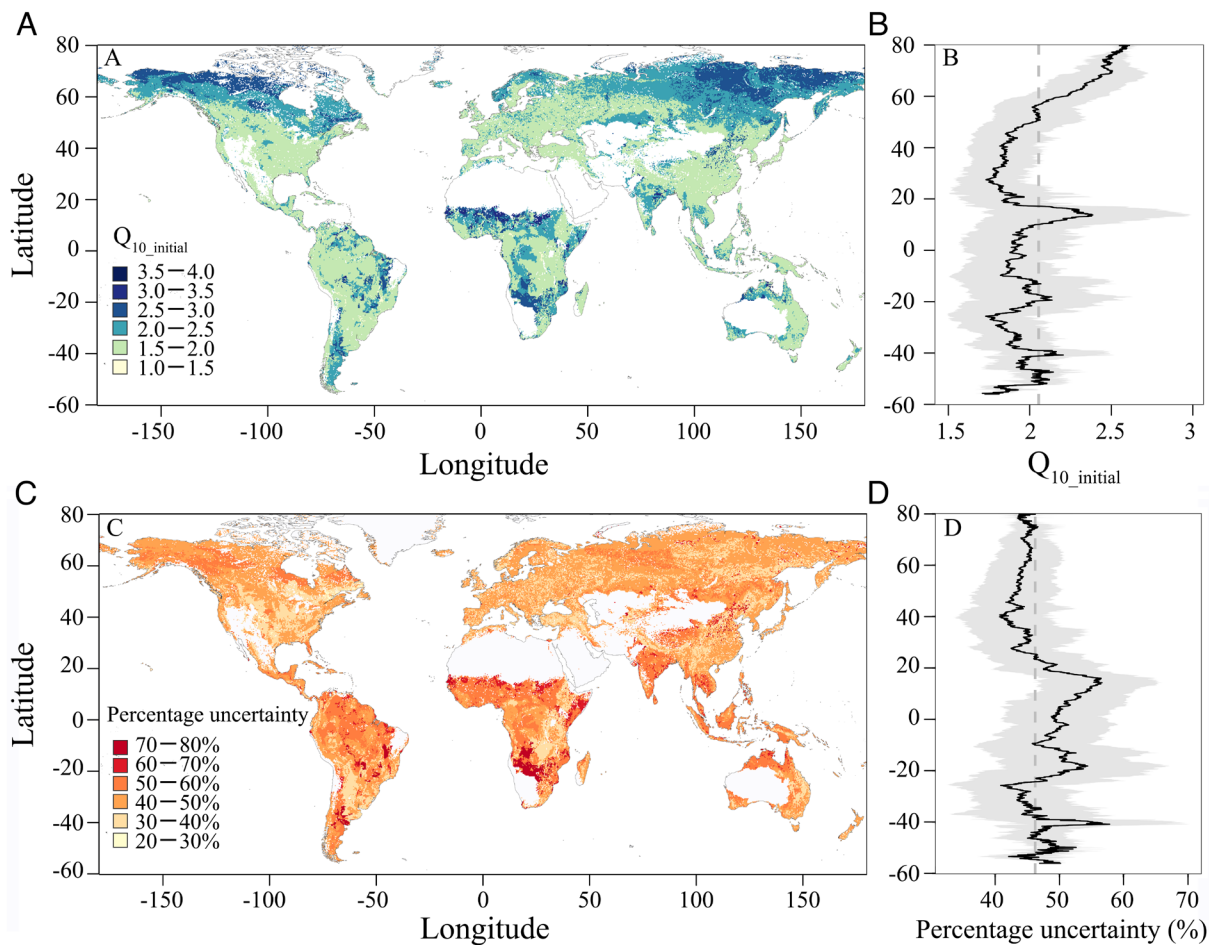


Fig. 5. Global spatial pattern of Q_{10} at the start of incubation ($Q_{10_initial}$) and its uncertainty. (A) and (B) $Q_{10_initial}$ and its latitudinal pattern, respectively. (C) and (D) Uncertainty of $Q_{10_initial}$ and its latitudinal pattern, respectively. Gray area in (B) and (D) shows one SD of the mean. Gray dashed lines show the global mean $Q_{10_initial}$ and its uncertainty. Uncertainty is estimated as the coefficient of variance of 500 estimates in the random forest model for predicting $Q_{10_initial}$.

changes as it is substrate-limited and has low-quality substrates. If high-quality SOC declines due to global change such as warming (39), topsoil SOC may show higher sensitivity to warming than subsoil SOC, which has been confirmed by estimates based on synthesizing SOC measurements in global soil profiles (4) as well as by incubation experiments (24). However, if substrate availability limitation is relieved in subsoil, subsoil SOC would show higher temperature sensitivity than topsoil SOC. Increasing carbon inputs to deep soil layers (e.g., by growing deep-rooting plants), for example, has been suggested as an effective way to promote carbon sequestration (40). Under climate warming, however, increased carbon input would also relax availability limitations, particularly in subsoil layers, thereby enhancing decomposition and offsetting the benefit for carbon sequestration. The global mapping of Q_{10} can help diagnose hotspots of sensitive areas of SOC mineralization under global warming, promoting soil carbon sequestration and climate change mitigation by managing carbon quality and availability.

Materials and Methods

Data Sources. A global dataset of SOC mineralization ($\text{g CO}_2\text{-C kg}^{-1}\text{ SOC d}^{-1}$) measured under laboratory incubation conditions was compiled by searching the Web of Science and the Chinese National Knowledge Infrastructure (CNKI). Topic keywords "soil AND (respir* OR ((carbon OR C OR CO2 OR carbon dioxide OR organic matter OR OM) AND (flux OR efflux OR emission OR release OR loss OR mineralize* OR decompos*))) AND (temperature OR warm* OR cool*) AND (incubat* OR culture)" are used for the search. As a complementary, we also

screened five published papers synthesizing SOC mineralization data (41–45) to target publications which may be missed from our search. All publications must meet the following criteria: 1) the soil used for incubation is sampled from the mineral layer; 2) the same soil must be incubated under at least two temperatures under otherwise same incubation conditions, enabling the estimation of Q_{10} ; and 3) time-course SOC mineralization rates are reported or can be directly calculated from the reported data. All relevant numerical data were directly extracted from the publication, and data presented in figures were extracted using WebPlotDigitizer (46). Finally, we obtained 21,979 data points observed by incubating 721 soils across the globe (SI Appendix, Fig. S1) from 191 publications (SI Appendix, Table S3).

In the dataset, incubation temperature ranges from -10°C to 60°C , and incubation duration ranges from 1 to 924 d. We also extracted, if available, SOC content, soil pH, total nitrogen content, soil C:N ratio, soil bulk density, and texture of the incubated soils before incubation. If these variables are not reported (SI Appendix, Table S1), we extracted them from the Harmonized World Soil Database (47). Ecosystem type (i.e., cropland, desert, forest, grassland, tundra, and wetland), site location (longitude and latitude), and variables relating to incubation manipulation (e.g., incubation temperature and soil moisture) were also recorded. At each soil location, climate attributes were extracted from WorldClim (48).

Temporal Dynamics of Q_{10} . We calculated the "equal-carbon" Q_{10} proposed by Rey and Jarvis (20) which can reflect the changes of temperature sensitivity of SOC with time (43). Specifically, Q_{10} was calculated based on the time required to mineralize a defined fraction of SOC under two temperatures (19):

$$Q_{10} = \left(\frac{t_f}{t_h} \right)^{\frac{10}{h - T_f}} \quad [1]$$

where t_{T_i} and t_{T_h} are the time required to mineralize the defined fraction of SOC under incubation temperature of T_i and T_h , respectively. Considering SOC as a continuum, the fraction of mineralized (or respired) SOC was determined at continuous gradients with an interval of percentage respired SOC of 0.2% (i.e., 0 to 0.2%, 0.2 to 0.4%, 0.4 to 0.6%, ...), which represent a gradient of decreasing lability of SOC with the proceeding of incubation). Here, we note that mineralized fraction at the end of incubation in some experiments does not reach to 0.2% (due to very short incubation duration and low incubation temperature), and these experiments are excluded for the assessment (SI Appendix, Table S3). This approach assumes that a certain amount of mineralized SOC comes from a similar fraction of SOC when the soils are at different temperatures, and labile pools will decompose faster/earlier than passive pools (19).

A machine learning-based statistic model—random forest—was used to explore the drivers over the variability of Q_{10} across the trials. Partial dependence analysis was used to test the relationship between the predicted Q_{10} and explanatory variables across the entire range of possible values included in the random forest modeling. The considered drivers are shown in SI Appendix, Table S1. Before fitting the model, the variance inflation factor (VIF) method was used to minimize the multicollinearity of explanatory variables. The explanatory variables with a VIF value greater than 10 were excluded. We classified the explanation factors into four main groups: 1) climate conditions, 2) soil properties, 3) vegetation, 4) experimental manipulation (e.g., temperature range used to calculate Q_{10} : $T_h - T_i$, ΔT —the difference between T_i and mean annual temperature at soil sampling location). The specific explanatory variables in each group after minimizing the multicollinearity are shown in SI Appendix, Table S1. In addition, we included the respired fraction of SOC (i.e., RF) as a proxy to represent the availability and quality of SOC. Nonparametric Kruskal–Wallis test was used to determine the significant difference. The VIF analysis was conducted using the `check_collinearity` function in R package performance, the random forest analysis was performed using `randomForest` function in R package randomForest, the partial dependence analysis was conducted using partial function in R package pdp, and the Kruskal–Wallis test was conducted using `kruskalmc` function in R package pgirmess. All data analyses were performed in R version 4.0.3 (<https://cran.r-project.org/>).

Data-Model Integration. Recalling our hypotheses (Fig. 1), we assume that the temporal dynamics of Q_{10} in each trial are controlled by carbon quality when the substrate availability is not limited, while Q_{10} is mainly controlled by carbon availability when the substrate availability is limited. A general model aligning with such assumptions can be written as (18):

$$Q_{10} = Q_{10_max} \cdot f(A) \cdot f(Q), \quad [2]$$

where Q_{10_max} is the maximum potential Q_{10} without limitations of carbon quality and availability, $f(A)$ and $f(Q)$ are the reduction factor due to carbon availability and quality limitations, respectively.

The Michaelis–Menten and Arrhenius kinetics represent mainstream modeling of SOC mineralization as impacted by carbon availability and quality, respectively. Under a typical temperature, the Michaelis–Menten and Arrhenius kinetics can be respectively written as:

$$k_{MM} = V_{max} \cdot \frac{S}{K_m + S}, \quad [3]$$

$$k_{Arr} = A \cdot e^{-\frac{E_a}{R \cdot T}}, \quad [4]$$

where V_{max} is the maximum rate of enzymatic reaction at a given temperature, K_m is the Michaelis–Menten (half-saturation) constant, S is the substrate content, A is the pre-exponential factor, E_a is the activation energy, R is the gas constant ($8.314 \text{ J K}^{-1} \text{ mol}^{-1}$), and T is the temperature in Kelvin. As Q_{10} can be generally estimated as the ratio of mineralization rate under a higher temperature (T_h) to that under a lower temperature (T_i), the temperature sensitivity of k_{MM} ($Q_{k_{MM}}$) and k_{Arr} ($Q_{k_{Arr}}$) can be, respectively, calculated as:

$$Q_{k_{MM}} = \frac{V_{max_T_h}}{V_{max_T_i}} \cdot \frac{K_{m_T_i} + S}{K_{m_T_h} + S}, \quad [5]$$

$$Q_{k_{Arr}} = e^{\frac{E_a}{R} \cdot \frac{T_h - T_i}{T_i \cdot T_h}}, \quad [6]$$

where $V_{max_T_h}$ and $V_{max_T_i}$ are the V_{max} under temperature T_h and T_i , respectively, $K_{m_T_h}$ and $K_{m_T_i}$ are the K_m under T_h and T_i , respectively. Both S and E_a keep constant under different temperatures (10, 16). $Q_{k_{MM}}$ and $Q_{k_{Arr}}$ can be normalized to their potential maximum value to represent $f(A)$ and $f(Q)$, respectively:

$$f(A) = \frac{K_{m_T_i} + S}{K_{m_T_h} + S}, \quad [7]$$

$$f(Q) = e^{\frac{E_a - E_{crit}}{R} \cdot \frac{T_h - T_i}{T_i \cdot T_h}}, \quad [8]$$

where E_{crit} is the critical activation energy (kJ mol^{-1}) under which k_{Arr} reaches the maximum. With the proceeding of incubation, S is expressed as an exponential function of the respired fraction of SOC (RF) (SI Appendix, Fig. S11):

$$S = S_0 \cdot e^{-\alpha \cdot RF}, \quad [9]$$

where S_0 is the initial substrate availability (mg C kg^{-1} soil) at the start of the incubation, α is the decreasing rate of substrate availability with RF. This function models that substrate availability decreases with the proceeding of incubation. E_a is expressed as a logistic function of RF (SI Appendix, Fig. S11):

$$E_a = \frac{E_{a_0} \cdot E_{crit}}{E_{a_0} + (E_{crit} - E_{a_0}) \cdot e^{-\beta \cdot RF}}, \quad [10]$$

where E_{a_0} is the initial activation energy (kJ mol^{-1}) at the start of the incubation, β is the increasing rate of activation energy with RF.

We optimized the model to capture the temporal changes in Q_{10} calculated under the RF gradients for each trial as well as for their average using a differential evolution algorithm (49). Prior ranges of the eight parameters in the model are shown in SI Appendix, Table S2. The root mean squared error (RMSE) between modeled and observed Q_{10} was minimized to target the optimal parameters. Considering potential parameter equifinality and observation uncertainty (50), we repeated the optimization for 200 times independently to obtain 200 ensembles of model parameters. For each optimization, specifically, observations were sampled from the probability distribution function of observed Q_{10} assuming a normal distribution defined by their SD (σ) and mean (μ) at each measurement time point. For each trial and each parameter, the median of the 200 estimates was calculated for comparison purpose. The optimization was performed using the function `DEoptim` in the package `DEoptim` in R 4.0.3.

Inferring Initial Q_{10} and Global Digital Mapping. At the beginning of incubation, the Q_{10} ($Q_{10_initial}$) can be estimated by setting $RF = 0$ in Eqs. 9 and 10:

$$Q_{10_initial} = Q_{10_max} \cdot \frac{K_{m_T_i} + S_0}{K_{m_T_h} + S_0} \cdot e^{\frac{E_{a_0} - E_{crit}}{R} \cdot \frac{T_h - T_i}{T_i \cdot T_h}}. \quad [11]$$

Correspondingly, $f(Q)$ and $f(A)$ can be, respectively, estimated as:

$$f(A)_{initial} = \frac{K_{m_T_i} + S_0}{K_{m_T_h} + S_0}, \quad [12]$$

$$f(Q)_{initial} = e^{\frac{E_{a_0} - E_{crit}}{R} \cdot \frac{T_h - T_i}{T_i \cdot T_h}}. \quad [13]$$

We estimated $Q_{10_initial}$, $f(A)_{initial}$, and $f(Q)_{initial}$ for each of the 721 soils. The estimates of $Q_{10_initial}$ were compared with the Q_{10} values of soil respiration (including heterotrophic- Q_{10_Rh} and total respiration- Q_{10_Rs}) observed in the field reported in ref. 28 at both global and ecosystem levels.

A random forest model was trained and validated (10-fold cross-validation) to predict $Q_{10_initial}$. The similar techniques for controlling predictor collinearity as the model for interpreting Q_{10} in the section *Temporal Dynamics of Q_{10}* were used. To facilitate global scale application, the model only includes environmental predictor variables that are meaningful at field conditions (SI Appendix, Table S1). This may damage model performance but can provide more realistic estimates aligning with the purpose of inferring Q_{10} in situ. Especially, the temperature predictor in the model used mean annual temperature at the site location, soil depth was set to 0 (the depth of layer top) and 30 cm (the depth of layer bottom). The validated model was applied in each 1-km grid across the globe using relevant global mapping products of the predictor variables in the model (SI Appendix, Table S1). Prediction uncertainty was quantified by estimating the SD of predictions from 500 randomly drawn trees in the fitted random forest model. The model training and global mapping were performed in R 4.0.3. The relevant data and code have been provided (see *Data, Materials, and Software Availability* statements).

Data, Materials, and Software Availability. Data used to generate the results are deposited to figshare through: (51). The field Q_{10} data were obtained from (28). Code (R scripts) used to assess the data and generate the results are deposited to figshare through: (52).

ACKNOWLEDGMENTS. This study is financially supported by the National Natural Science Foundation of China (grant no. 32241036 and 32171639) and the National Key Research and Development Program of the Ministry of Science and Technology of China (grant no. 2021YFE0114500). We thank Xiali Mao, Shengyao Jia, Tian Qian, Tong Jiang, Yin Lin, Yaoyao Chen, Shuxun Cheng, Zhuolin Yu, Min Wang for assisting data collection.

Author affiliations: ^aInstitute of Applied Remote Sensing and Information Technology, College of Environmental and Resource Sciences, Zhejiang University, Hangzhou 310058, China; ^bNational Engineering and Technology Center for Information Agriculture, Nanjing Agricultural University, Nanjing 210095, China; ^cInstitute of Ecology, College of Urban and Environmental Sciences, Peking University, Beijing 100871, China; ^dAcademy of Ecological Civilization, Zhejiang University, Hangzhou 310058, China; and ^eKey Laboratory of Environment Remediation and Ecological Health, Ministry of Education, Zhejiang University, Hangzhou 310058, China

- R. A. Houghton, The contemporary carbon cycle. *Treat. Geochem.* **8**, 473–513 (2003).
- X. Tang *et al.*, Spatial and temporal patterns of global soil heterotrophic respiration in terrestrial ecosystems. *Earth Syst. Sci. Data* **12**, 1037–1051 (2020).
- B. Bond-Lamberty, V. L. Bailey, M. Chen, C. M. Gough, R. Vargas, Globally rising soil heterotrophic respiration over recent decades. *Nature* **560**, 80–83 (2018).
- M. Wang *et al.*, Global soil profiles indicate depth-dependent soil carbon losses under a warmer climate. *Nat. Commun.* **13**, 1–11 (2022).
- T. W. Crowther *et al.*, Quantifying global soil carbon losses in response to warming. *Nature* **540**, 104–108 (2016).
- M. U. F. Kirschbaum, The temperature dependence of organic-matter decomposition—still a topic of debate. *Soil Biol. Biochem.* **38**, 2510–2518 (2006).
- L. L. Reynolds, K. Lajtha, R. D. Bowden, B. R. Johnson, S. D. Bridgman, The carbon quality-temperature hypothesis does not consistently predict temperature sensitivity of soil organic matter mineralization in soils from two manipulative ecosystem experiments. *Biogeochemistry* **136**, 249–260 (2017).
- E. Bosatta, G. I. Ågren, Soil organic matter quality interpreted thermodynamically. *Soil Biol. Biochem.* **31**, 1889–1891 (1999).
- E. A. Davidson, I. A. Janssens, Temperature sensitivity of soil carbon decomposition and feedbacks to climate change. *Nature* **440**, 165–173 (2006).
- S. Arrhenius, Über die Reaktionsgeschwindigkeit bei der Inversion von Rohrzucker durch Säuren. *Zeitschrift für physikalische Chemie* **4**, 226–248 (1889).
- J. M. Craine, N. Fierer, K. K. McLauchlan, Widespread coupling between the rate and temperature sensitivity of organic matter decay. *Nat. Geosci.* **3**, 854–857 (2010).
- M. A. Bradford *et al.*, Thermal adaptation of soil microbial respiration to elevated temperature. *Ecol. Lett.* **11**, 1316–1327 (2008).
- J. M. Melillo *et al.*, Soil warming and carbon-cycle feedbacks to the climate system. *Science* **298**, 2173–2176 (2002).
- L. L. Liang, M. U. Kirschbaum, V. L. Arcus, L. A. Schipper, The carbon-quality temperature hypothesis: Fact or artefact? *Glob. Change Biol.* **29**, 935–942 (2022).
- J. Eberwein, P. Oikawa, L. Allsman, G. Jenerette, Carbon availability regulates soil respiration response to nitrogen and temperature. *Soil Biol. Biochem.* **88**, 158–164 (2015).
- A. Gershenson, N. E. Bader, W. Cheng, Effects of substrate availability on the temperature sensitivity of soil organic matter decomposition. *Glob. Change Biol.* **15**, 176–183 (2009).
- J. A. Dungait, D. W. Hopkins, A. S. Gregory, A. P. Whitmore, Soil organic matter turnover is governed by accessibility not recalcitrance. *Glob. Change Biol.* **18**, 1781–1796 (2012).
- E. A. Davidson, S. Samanta, S. S. Caramori, K. Savage, The Dual Arrhenius and Michaelis-Menten kinetics model for decomposition of soil organic matter at hourly to seasonal time scales. *Glob. Change Biol.* **18**, 371–384 (2012).
- R. T. Conant *et al.*, Sensitivity of organic matter decomposition to warming varies with its quality. *Glob. Change Biol.* **14**, 868–877 (2008).
- A. Rey, P. Jarvis, Modelling the effect of temperature on carbon mineralization rates across a network of European forest sites (FORCAST). *Glob. Change Biol.* **12**, 1894–1908 (2006).
- I. P. Hartley, T. C. Hill, S. E. Chadburn, G. Hugelius, Temperature effects on carbon storage are controlled by soil stabilisation capacities. *Nat. Commun.* **12**, 6713 (2021).
- M. D. Wallenstein, S. D. Allison, J. Ernakovich, J. M. Steinweg, R. L. Sinsabaugh, "Controls on the temperature sensitivity of soil enzymes: A key driver of in situ enzyme activity rates" in *Soil Enzymology*, G. Shukla, A. Varma, Eds. (Springer, 2011), pp. 245–258.
- X. Mao *et al.*, Climate-induced shifts in composition and protection regulate temperature sensitivity of carbon decomposition through soil profile. *Soil Biol. Biochem.* **172**, 108743 (2022).
- S. Qin *et al.*, Temperature sensitivity of SOM decomposition governed by aggregate protection and microbial communities. *Sci. Adv.* **5**, eaau1218 (2019).
- J. Leifeld, M. von Lütow, Chemical and microbial activation energies of soil organic matter decomposition. *Biol. Fert. Soils* **50**, 147–153 (2014).
- L. Henneron *et al.*, Bioenergetic control of soil carbon dynamics across depth. *Nat. Commun.* **13**, 7676 (2022).
- J. M. Melillo *et al.*, Long-term pattern and magnitude of soil carbon feedback to the climate system in a warming world. *Science* **358**, 101–105 (2017).
- D. Haaf, J. Six, S. Doetterl, Global patterns of geo-ecological controls on the response of soil respiration to warming. *Nat. Clim. Chang.* **11**, 623–627 (2021).
- S. D. Allison, M. D. Wallenstein, M. A. Bradford, Soil-carbon response to warming dependent on microbial physiology. *Nat. Geosci.* **3**, 336–340 (2010).
- E. A. Davidson, I. A. Janssens, Y. Luo, On the variability of respiration in terrestrial ecosystems: Moving beyond Q_{10} . *Glob. Change Biol.* **12**, 154–164 (2006).
- M. C. Mack, E. A. Schuur, M. S. Bret-Harte, G. R. Shaver, F. S. Chapin III, Ecosystem carbon storage in arctic tundra reduced by long-term nutrient fertilization. *Nature* **431**, 440–443 (2004).
- J. P. Schimel, C. Bilbrough, J. M. Welker, Increased snow depth affects microbial activity and nitrogen mineralization in two Arctic tundra communities. *Soil Biol. Biochem.* **36**, 217–227 (2004).
- M. D. Wallenstein, S. K. McMahon, J. P. Schimel, Seasonal variation in enzyme activities and temperature sensitivities in Arctic tundra soils. *Glob. Change Biol.* **15**, 1631–1639 (2009).
- J. Limpens *et al.*, Peatlands and the carbon cycle: From local processes to global implications—a synthesis. *Biogeosciences* **5**, 1475–1491 (2008).
- F. E. Moyano, M. Manzoni, C. Chenu, niubi Responses of soil heterotrophic respiration to moisture availability: An exploration of processes and models. *Soil Biol. Biochem.* **59**, 72–85 (2013).
- L. Xiao *et al.*, Younger carbon dominates global soil carbon efflux. *Glob. Change Biol.* **28**, 5587–5599 (2022).
- L. Liu, J. S. King, C. P. Giardina, Effects of elevated concentrations of atmospheric CO₂ and tropospheric O₃ on leaf litter production and chemistry in trembling aspen and paper birch communities. *Tree Physiol.* **25**, 1511–1522 (2005).
- J. Balesdent *et al.*, Atmosphere–soil carbon transfer as a function of soil depth. *Nature* **559**, 599–602 (2018).
- T. Ise, A. L. Dunn, S. C. Wofsy, P. R. Moorcroft, High sensitivity of peat decomposition to climate change through water-table feedback. *Nat. Geosci.* **1**, 763–766 (2008).
- N. A. Eckardt *et al.*, Climate change challenges, plant science solutions. *Plant Cell* **35**, 24–66 (2022).
- N. Fierer, P. P. Colman, J. P. Schimel, R. B. Jackson, Predicting the temperature dependence of microbial respiration in soil: A continental-scale analysis. *Glob. Biogeochem. Cycles* **20**, GB3026 (2006).
- C. Schädel *et al.*, Decomposability of soil organic matter over time: The Soil Incubation Database (SIDb, version 1.0) and guidance for incubation procedures. *Earth Syst. Sci. Data* **12**, 1511–1524 (2020).
- S. Hamdi, F. Moyano, S. Sall, M. Bernoux, T. Chevallier, Synthesis analysis of the temperature sensitivity of soil respiration from laboratory studies in relation to incubation methods and soil conditions. *Soil Biol. Biochem.* **58**, 115–126 (2013).
- S. Ren *et al.*, Higher temperature sensitivity of soil C release to atmosphere from northern permafrost soils as indicated by a meta-analysis. *Glob. Biogeochem. Cycles* **34**, e2020GB006688 (2020).
- Q. Wang *et al.*, Global synthesis of temperature sensitivity of soil organic carbon decomposition: Latitudinal patterns and mechanisms. *Funct. Ecol.* **33**, 514–523 (2019).
- B. U. Burda, E. A. O'Connor, E. M. Webber, N. Redmond, L. A. Perdue, Estimating data from figures with a Web-based program: Considerations for a systematic review. *Res. Synth. Methods* **8**, 258–262 (2017).
- Food and Agriculture Organization (FAO). Harmonized world soil database (version 1.2) (FAO, Rome, 2012).
- S. E. Fick, R. J. Hijmans, WorldClim 2: New 1-km spatial resolution climate surfaces for global land areas. *Int. J. Climatol.* **37**, 4302–4315 (2017).
- K. Mullen, D. Ardia, D. L. Gil, D. Windover, J. Cline, DEoptim: An R package for global optimization by differential evolution. *J. Stat. Softw.* **40**, 1–26 (2011).
- Z. Luo, Z. Tang, X. Guo, J. Jiang, O. J. Sun, Non-monotonic and distinct temperature responses of respiration of soil microbial functional groups. *Soil Biol. Biochem.* **148**, 107902 (2020).
- S. Zhang *et al.*, Data from "Reconciling carbon quality with availability predicts temperature sensitivity of global soil carbon mineralization." Figshare. <https://doi.org/10.6084/m9.figshare.22817525.v1>. Deposited 14 May 2023.
- S. Zhang *et al.*, Code from "Reconciling carbon quality with availability predicts temperature sensitivity of global soil carbon mineralization." Figshare. <https://doi.org/10.6084/m9.figshare.22817519.v1>. Deposited 14 May 2023.